# Xrs2/NBS1 promote end-bridging activity of the MRE11-RAD50 complex

(article starts on next page)

# Xrs2/NBS1 promote end-bridging activity of the MRE11-RAD50 complex

Carl Möller [a],[1], Rajhans Sharma [a],[1], Robin Öz [a], Giordano Reginato [b], Elda Cannavo [b], Ilaria Ceppi [b], Sriram K.K. [a], Petr Cejka [b],[c], Fredrik Westerlund [a],[*]

[a] *Department of Life Sciences, Chalmers University of Technology, Gothenburg, SE, 41296, Sweden*
[b] *Institute for Research in Biomedicine, Universitá della Svizzera Italiana, Bellinzona, CH 6500, Switzerland*
[c] *Department of Biology, Institute of Biochemistry, Eidgenössische Technische Hochschule (ETH) Zürich, Switzerland*

## ARTICLE INFO

## ABSTRACT

DNA double strand breaks (DSBs) can be detrimental to the cell and need to be efficiently repaired. A first step in DSB repair is to bring the free ends in close proximity to enable ligation by non-homologous end-joining (NHEJ), while the more precise, but less available, repair by homologous recombination (HR) requires close proximity of a sister chromatid. The human MRE11-RAD50-NBS1 (MRN) complex, Mre11-Rad50-Xrs2 (MRX) in yeast, is involved in both repair pathways. Here we use nanofluidic channels to study, on the single DNA molecule level, how MRN, MRX and their constituents interact with long DNA and promote DNA bridging. Nanofluidics is a suitable method to study reactions on DNA ends since no anchoring of the DNA end(s) is required. We demonstrate that NBS1 and Xrs2 play important, but differing, roles in the DNA tethering by MRN and MRX. NBS1 promotes DNA bridging by MRN consistent with tethering of a repair template. MRX shows a "synapsis-like" DNA end-bridging, stimulated by the Xrs2 subunit. Our results highlight the different ways MRN and MRX bridge DNA, and the results are in agreement with their key roles in HR and NHEJ, respectively, and contribute to the understanding of the roles of NBS1 and Xrs2 in DSB repair.

## 1. Introduction

The information stored in our genome needs to be preserved during both programmed cellular processes and spontaneous events that give rise to DNA double strand breaks (DSBs). Although DSBs occur at a much lower frequency than other types of DNA damage, they are one of the most cytotoxic lesions [1,2]. Eukaryotes have a functional DNA damage response (DDR) network that is capable of cell cycle regulation, signal transduction and DNA repair in response to compromised genome integrity. Central to DDR in human cells are the key signaling and repair proteins MRE11, RAD50 and NBS1 that together form the MRN complex [3]. The MRE11-RAD50 (MR) subcomplex is conserved across several domains of life, whereas NBS1 (with its homologue Xrs2 in *S. cerevisiae*) is conserved only in eukaryotes. MRN/X is one of the first protein complexes that is recruited to DSBs, where it initiates repair through ATM/Tel1 activation, DNA end resection, and tethering of the DNA ends in close proximity for repair [3,4]. Depending on the type of DNA lesion and the cell cycle stage, MRN/MRX channels the repair to either Homologous Recombination (HR), Non-Homologous End Joining (NHEJ) or Micro-homology Mediated End-Joining (MMEJ) [5,6].

The MRN/X complex has three domains, the globular head, a 'coiled-coil', and a 'hook' at the apex of the coils. MRE11 homodimerizes to form the center of the globular head bound between the N-terminal domain of NBS1/Xrs2 and two RAD50 entitites [7,8]. The nuclease domains of MRE11 consist of five conserved phosphodiesterase motifs that bind DNA and are responsible for the nuclease activity [9–14]. The coiled-coil domain belongs to the RAD50 subunit and can dimerize either inter- or intramolecularly through its zinc-mediated CXXC motif at the apex of the 'coiled-coil', giving rise to the hook domain [15]. The N- and C-terminal domains of RAD50 have ATP-binding subunits that are relatively relaxed, or open, in the ATP-hydrolyzed state [16,17]. Upon ATP binding, both the terminals of RAD50 come in contact with each other, forming a rigid conformation that can accommodate a DNA double strand in the grove [16–18]. During the initial steps of HR, the MRN/X complex associates with phosphorylated CtIP in mammals (Sae2 in yeast) to promote the endonuclease activity of MRE11 [19,20]. Such DNA cleavage is particularly important if the DNA ends are blocked with secondary structures or proteins (such as the NHEJ factor Ku) [21,22].

---

DNA end resection is generally only permissible during the S and G2 phases of the cell cycle when sister chromatids are available. CtIP/Sae2 are in this context targets of cyclin-dependent kinases (CDKs) and are also subject to phosphorylation by ATM/Tel1 in a DNA damage-dependent manner [23].

The NBS1/Xrs2 protein is the least conserved subunit that markedly differs in structure and functionality between organisms and is also the least understood [19]. The N-terminal domain of both NBS1 and Xrs2 has a fork head associated (FHA) domain that binds phosphorylated XRCC4/Lif1 and CtIP/Sae2, respectively [24]. While NBS1 is essential for DNA end resection [25], Xrs2 is largely dispensable [26]. Furthermore, a recent study found that NBS1 can sense phosphorylated CtIP via its BRCA1 C-terminal (BRCT) domain, a structural feature that Xrs2 does not have [25]. Both NBS1 and Xrs2 share an MRE11 binding domain as well as a Tel1/ATM binding domain, and consequently both NBS1 and Xrs2 are essential for Tel1/ATM activation. Towards the C-terminal end, both NBS1 and Xrs2 have a nuclear localization sequence (NLS) that is required for nuclear import [7,27–29]. Studies have shown that decreased DNA damage sensitivity in *xrs2Δ* cells can be partially rescued by fusing Mre11 to an NLS, but DNA repair by NHEJ cannot, indicating the importance of Xrs2 in NHEJ [29,30]. Additionally, Mre11-NLS *xrs2Δ* cells showed significantly decreased DNA-tethering and replication fork stability [29]. The importance of Xrs2 in DNA-tethering is further highlighted by findings showing that MRX has a significant role in increasing the tethering and subsequent ligation of DNA ends by Dnl4/Lif1, but yeast Mre11 on its own does not [31]. Interestingly, comparable experiments with human MRE11 and MRN together with Ligase IV/XRCC4 have shown that neither MRE11 nor MRN is sufficient to promote the ligation of broken ends *in vitro* [14,32,33]. This, together with results showing that NBS1 deficient cells generate NHEJ events at the same level as wild type cells but have a significant decrease in HR frequency [34,35], indicates the lesser involvement of NBS1 in NHEJ and highlights the importance in HR and ATM activation.

Single molecule techniques are important tools when investigating protein-DNA interaction since they can reveal protein functions that are hidden in bulk experiments [36,37]. Single molecule studies of MRE11 complexes (MR, MRN/X) have provided insights into their function and yielded detailed information regarding structural mechanisms governing these functions [38–40]. In a recent study, DNA curtains were used to determine the rate of removal of the DNA dependent protein kinase (DNA-PK) from DNA by the MRN/CtIP complex. It was concluded that MRN diffuses in a 1D manner along the DNA to find the broken ends, and that MRN is dependent on DNA-PK and phosphorylated CtIP for efficient processing and resection of DNA ends [41,42]. Atomic Force Microscopy (AFM) studies have revealed that human MR complexes can tether and join DNA ends by loading the MRE11 dimer on the DNA, creating inter-complex interactions through the zinc-hook on the coiled-coil of RAD50 [38,39,43]. Importantly, the tethering by MR seems to be only stable when sufficiently many MR protein complexes are present [38]. Similar observations have been made for archaeal MR [40]. It has also been shown that RAD50 can bind DNA, but not tether it, although complexes of RAD50 and NBS1 can [44,45]. A recently determined structure of MRN confirms the role of the RAD50 coiled-coils in inter-complex interactions and the possibility of a stabilizing role of NBS1 in DNA tethering [46]. MR can bind either at the DNA ends or anywhere along the DNA contour, where the globular head of MR interacts with the DNA and the coiled-coils of RAD50 extend from the DNA substrate [17,47–50]. At increased concentrations of MR, higher order structures like loops, bridges and end tethers have also been observed [51,52]. Interestingly, Xrs2 itself has an intrinsic DNA binding activity and recognizes single stranded overhangs on linear DNA [53], which has not yet been reported for NBS1.

An inherent limitation with most single molecule techniques for studying proteins interacting with DNA, in particular for long DNA, is that they rely on anchoring the DNA end(s) to a surface. This in turn restricts the possibilities of studying interactions that occur on DNA ends, and more importantly, it makes the study of connecting DNA ends, a key process in many reactions in DSB repair and genome maintenance, more difficult. Nanofluidic channels, on the other hand, have during the last years emerged as a powerful tool to study DNA-protein interactions [54,55] where the trapping and confinement of DNA in nanochannels stretches the molecule without anchoring the DNA. This makes the method particularly useful for studying reactions that need free DNA ends to interact [56]. Of most relevance here is a recent study on the DNA bridging capabilities of the MRN and MRX co-factors CtIP and Sae2 [57]. We observed that when mixing CtIP with λ-DNA, that has complementary single stranded overhangs, a large fraction of circular DNA was formed. We interpreted this as being due to CtIP bridging distant regions of DNA and promoting intramolecular annealing of the overhangs. Sae2, on the other hand, preferably promoted intermolecular bridging [57].

In this work we further explored the capabilities of nanofluidic channels as a tool for studies of protein-DNA interaction by characterizing how the MRN and MRX complexes, and their constituents, interact with a long DNA substrate and bridge DNA ends. We took a similar approach as in our previous study on CtIP [57], where thousands of protein-DNA complexes were imaged at each condition. From the extracted kymographs we obtained information on the DNA conformation and details regarding local features along each DNA molecule. By mapping the different conformational populations, we could determine a significant difference in how MRN and MRX bridge DNA ends. While MRN showed a strong tendency to bridge DNA in an intramolecular manner, where the ends of a single DNA molecule hybridize to generate a circular conformation, MRX showed a behavior which rather can be explained by tethering of the ends of neighboring DNA molecules, which generates long concatemers consisting of multiple DNA segments. Interestingly, we found that this difference can be partially explained by the ways that NBS1 and Xrs2 subunits bridge DNA. We believe that these findings provide valuable insights into the initial steps of DSB repair and further strengthen the importance and universality of the MRN/X complex in genome stability.

## 2. Materials and methods

### 2.1. Protein purification

The recombinant MRX complex was expressed in *Spodoptera frugiperda* 9 (*Sf*9) cells using constructs for His-tagged Mre11, FLAG-tagged Xrs2 and untagged Rad50 and purified by affinity chromatography as described previously [58]. The yeast Mre11-Rad50 complex was purified by affinity chromatography and ion-exchange chromatography in *Sf*9 cells with constructs for His-tagged Mre11 and untagged Rad50 as described previously [26]. Recombinant phosphorylated Xrs2 was expressed in Sf9 cells and purified by FLAG affinity chromatography as previously described [29] with the following modifications: 100 nM okadaic acid (final concentration, Calbiochem) was added to the Sf9 culture 3 h prior to the harvesting. Additionally, the lysis buffer was supplemented with the following phosphatase inhibitors to preserve protein phosphorylation: 1 mM EDTA (Sigma), 100 nM okadaic acid, 1 mM Na3VO4 (Sigma), 20 mM NaF (Applichem), and 15 mM Na4P2O7 (Applichem). The human MRN or MR complexes were expressed in Spodoptera frugiperda Sf9 cells with constructs for His-tagged MRE11, FLAG-tagged RAD50 and untagged NBS1 and purified using affinity chromatography and ion exchange chromatography as described previously [25,59]. MBP-NBS1-His was expressed in Sf9 cells and purified as described previously [25].

### 2.2. Nanofluidic device

The nanofluidic device was fabricated in oxidized silicon as described elsewhere [60]. The nanofluidic device used in this study is depicted in Fig. 1A together with examples of confined molecules and
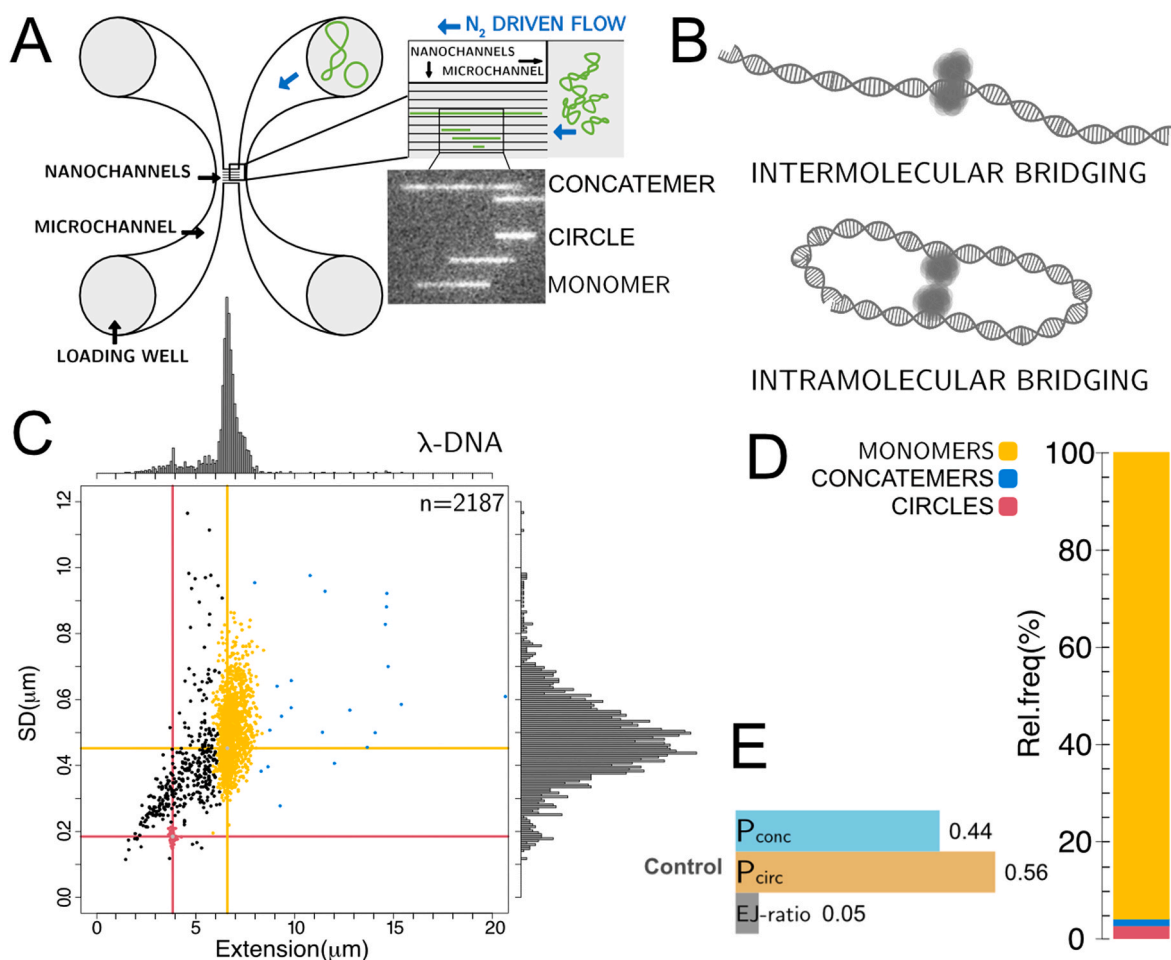
**Fig. 1.** **A)** Schematic of the nanofluidic chip used for confining and imaging of DNA molecules. Examples of molecules show how different conformations can appear during imaging. A circular DNA molecule will appear shorter and brighter compared to a monomeric linear molecule while a concatemer will be longer. **B)** Cartoon showing the two types of bridging events that can occur when the single stranded overhangs of λ-DNA hybridize. Hybridization with a neighboring molecule will generate concatemers, *intermolecular bridging*, which will be n-times the length of a monomeric λ-DNA, while hybridization of the ends of the same molecule, *intramolecular bridging*, will close the λ-DNA into a circle. **C)** Scatterplot from a control sample of λ-DNA showing the extension versus the standard deviation of the extension. Each point represents a molecule, and the colors represent molecules that have been categorized as belonging to one of the conformational populations. Black points are molecules that fall outside the categories due to being e.g., damaged etc. **D)** Relative abundance of the different conformational populations found in a λ-DNA (N = 2187) control sample. **E)** "end-joining" ratio for control sample with λ-DNA. The EJ ratio is the relation between the number of observed monomers and the number of end-joining events where the number of end-joining events is based on the number of circles plus the number of monomers found in concatemers. A low ratio indicates a low number of "end-joing events" per observed monomer. A ratio > 1 indicates that there are more observed "end-joining events" than monomers. (For interpretation of the references to color in this figure legend, the reader is referred to the Web version of this article.)

insets describing the stretching of a DNA molecules in a nanochannel. The device, in short, consist of two parallel microfluidic channels that are connected by a grid of nanochannels into which the molecules of interest are driven by a hydrodynamic flow induced by pressurized nitrogen gas. The nanochannels are 100 nm deep, 150 nm wide and 500 μm long. Before using the nanofluidic device for experiments they were thoroughly cleaned by flushing once with SDS (10 % w/w) solution and then three times with milli-Q water until thoroughly cleaned.

### 2.3. Sample preparation

The linear bacteriophage lambda-DNA (λ-DNA, 48.5 kbp) was purchased from Roche and diluted to working concentrations in the incubation buffer described below. All experiments were carried out at a final DNA concentration of 4 μM (base pairs), unless otherwise specified. The desired molar ratios of DNA and protein were incubated at 30 °C or 37 °C for 1 h in incubation buffer (10 mM TRIS, pH 7.6, 10 mM NaCl, 5 mM DTT). The DNA staining dye YOYO-1 (Invitrogen) was added to the incubated sample at a ratio of 5 bp to 1 (DNA:YOYO) and further

incubated for 15 min at room temperature before loading into the device. A total of 10 μL of incubated DNA or DNA-protein complex sample was loaded into one of the reservoirs and the remaining three reservoirs were filled with the incubation buffer. A final concentration of 0.05% w/v SDS was added to the reaction prior to loading on the nanofluidic chip in order to reduce non-specific sticking of complexes to the channel walls [57]. While the addition of a detergent such as SDS is normally detrimental for proteins the majority of the added SDS molecules are expected to coat the channel walls which reduces the number of available molecules in solution significantly.

### 2.4. Nanofluidic experiments

The DNA sample was driven from the reservoirs through either microchannel using a hydrodynamic flow driven by pressurized nitrogen gas. To introduce the DNA molecules from the microchannels into the nanochannels, pressure was applied to both reservoirs at the ends of the microchannel. To collect the maximum number of molecules during imaging, the DNA molecules were first carefully pushed to accumulate

in sufficient numbers at the entrance of the nanochannels. This was done by opening the pressure from both reservoirs on the same side of the nanochannels for ~10 s. After that, these concentrated DNA molecules were pushed into the nanochannels. Between 60 and 100 molecules were imaged in each field of view. Once in the nanochannels, the DNA molecules were allowed to equilibrate for 15 s before imaging. Imaging was done using a fluorescence microscope (Zeiss AxioObserver.Z1) equipped with a 63 × (1.6 × optovar) oil immersion objective (NA = 1.46, Zeiss) and a Photometrics Prime95B EMCCD camera. For excitation a Zeiss Colibri 7 LED was used and set to 469 nm coupled with Filterset 44 FITC (Zeiss). The Zen pro software was used to capture 50 frames with an exposure time of 100 ms.

### 2.5. Experiments on glass slides

Glass coverslips were functionalized to become positively charged as described elsewhere [61,62]. In short, the glass coverslips are first sonicated in KOH and acetone to remove any contaminants. After drying with nitrogen gas the glass coverslips were submerged in a 1% (v/v) mixture of Allyltrimethoxysaline (ATMS) and (3-Aminopropyl) trimethoxysilane (APTES) mixed in acetone for a minimum of 2 h. This generated a self-assembled monolayer with a net positive charge, allowing the negatively charged DNA to interact with the surface. Prior to adding the sample, the coverslips were washed in MQ water to remove the acetone and dried under nitrogen gas. DNA and protein samples was prepared in the same way as in the nanofluidics assay. Additionally, aptamer coated QDOTS were added to the protein-DNA reaction in order to provide a way to localize proteins bound to the DNA [63,64]. In short, a biotin tagged 6xHis-tag specific aptamer [65] was diluted, boiled, and cooled on ice in its selection buffer to fold properly. The aptamer was then added in 5 times excess to streptavidin conjugated Qdot™ 6 55(Q10123MP, ThermoFischer Scientific) and incubated for 10 min at room temperature. The complex was subsequently added to the DNA-protein sample and incubated for an additional 10 min. The reaction was diluted further to get a proper density of molecules on the glass surface for imaging. Next the DNA-protein complexes were deposited on the modified glass substrate by applying the sample to the edge of the sandwiched glass slide and coverslip. This generates capillary forces that drag the liquid across the surfaces to deposits the DNA in a stretched-out configuration. The sample was then imaged with a inverted fluorescence microscope (Zeiss AxioObserver. Z1) equipped with a 63x oil immersion objective (NA = 1.46, Zeiss), 1.6 × optovar magnification changer, an iXon EMCCD camera (Andor) and a LDI-7 Laser Diode Illuminator (89 NORTH). For excitation either 640n m or 470 nm light was used to excite the sample and the subsequent emission was passed through Filterset 50 Cy5 or 44 FITC(Zeiss) before reaching the detector. See Supplementary Figs. 1–4 for a full description and complementary data.

### 2.6. Data analysis

All data analysis was performed using custom-written MATLAB or R-based scripts. The extension and corresponding standard deviation ($STD_{Ext}$) for each DNA-protein complex was extracted from the kymograph, generated from the recorded image stack [66].

#### 2.6.1. Conformation classification and relative populations

After the average extension and the standard deviation was extracted from each kymograph a scatterplot was generated with the distribution displayed along each axis, see Fig. 1C. From the peaks in the histograms of both the $STD_{Ext}$ and the extension it was determined where the highest density areas were located along each axis and thus potential major clusters. The location of the peaks gave the center of each high-density area and the full width at half-max of each peak was used to set boundaries within which clusters most likely would be situated. The peaks and their width were then used to define an area on the scatterplot

within which the center of each conformation category would lie. To categorize the molecules, Euclidean distance hierarchical clustering was used to generate 100 small clusters. The individual clusters were assigned to a category if > 2/3 of the cluster members were situated within the boundaries defined according to the above. The circular fraction was found via the same method as the monomeric fraction, with the boundaries set to the intersection of high-density $STD_{Ext}$ peaks below the main monomeric peak and an extension around 1/2 of the linear (*λ-DNA monomer*) molecule fraction [57]. The initial position of the linear fraction was estimated from control data where an absolute majority of the molecules are expected to fall in this category. Concatemers where defined as molecules with an extension higher than $max_{EXT}$ of the linear fraction. Molecules falling below the $min_{EXT}$ of the linear fraction but had a $STD_{Ext}$ above $max_{STD}$ of the circular fraction are categorized as "fragments" since a majority of these are broken linear molecules. These molecules are excluded when determining the relative populations, Fig. 1D, which are calculated according to $\frac{category}{circles+concatemers+monomers}$. The relative populations reported in Fig. 3D–E and Fig. 4A–B, D are based on at least three technical replicates for each condition. Each replicate was analyzed as described above and a mean value for each population was calculated as well as the standard deviation of that mean to indicate the spread across the replicates. The standard deviation is visualized with error bars for each condition.

#### 2.6.2. "End-joining" ratio

The "end-joining" (EJ) ratio is a relative number describing the likelihood of a molecule being part of an "end-joining event". This is defined as the hybridisation of two DNA ends and includes both the formation of circles and concatemers. The EJ-ratio is based on the number of EJ-events and the total number of observed λ-DNA molecules, where a molecule categorized as monomer or circle consists of one λ-DNA molecule while concatemers are weighted based on the number of λ-DNA monomers in the concatemer. "EJ.ratio" for all conditions are reported in Supplementary Table 3 together with "$P_{circ}$", "$P_{conc}$" and the number of monomers, circles and concatemers used for calculations. "$P_{circ}$" is the likelihood of an EJ event being circularization while "$P_{conc}$" is the equivalent for concatemer formation.

### 2.7. EMSA

Electromobility shift assays (EMSA) with the yeast proteins were done by mixing protein and 100 ng linearized pUC19 (EcoRI) in 25 mM Tris-OAc, 1 mM DTT, 2 mM EDTA, 50 µg/µl bovine serum albumin (BSA)(New England Biolabs), where indicated, 2 mM MgOAc and 1 mM ATPγS was also included. Electromobility shift assay (EMSA) with the human proteins were performed as indicated above with the exception that 0.25 mg/ml BSA (NEB) was used. The reactions were incubated on ice for 30 min and loaded on a 0.6% agarose gel. The results were quantified by selecting the area where free DNA could be observed in the control sample and applying the mask on all other samples, summing up the pixel intensity within the area. The same was done for the remaining area of the lane. The relative summed pixel intensity of each area, either for free or bound DNA, was calculated to get a comparable number of how much the amount of free or bound DNA had changed in relation to the control sample for each lane.

### 2.8. Nuclease assay

The substrate for the endonuclease assay was prepared by annealing 3′-labeled oligonucleotide PC210 with a two-fold excess of complementary PC211 as described previously [67]. The radioactive nuclease assays (15 µl volume) were assembled on ice in reaction buffer containing 25 mM Tris-acetate (pH 7.5), 1 mM DTT, 5 mM magnesium acetate, 1 mM manganese acetate, 1 mM ATP, 80 U/ml pyruvate kinase (Sigma), 1 mM phosphoenolpyruvate, 0.25 mg/ml bovine serum

albumin (New England Biolabs), and 1 nM (in molecules) DNA substrate. The reactions were supplemented with 30 nM Streptavidin (Sigma) and incubated for 5 min at room temperature, then returned on ice. Subsequently, the relevant proteins were added, and the reactions were incubated for 30 min at 30 °C. The reactions were stopped by the addition of 0.5 μl of 14–22 mg/ml proteinase K (Roche), 0.5 μl of 10% (w/v) sodium dodecyl sulfate, and 0.5 μl of 0.5 M ethylenediaminetetraacetic acid (EDTA) pH 8.0 for 30 min at 50 °C and then mixed with an equal volume of loading dye (95% formamide, 20 mM EDTA, 1 mg/ml bromophenol blue). The products were analyzed by denaturing electrophoresis on 15% polyacrylamide gels (acrylamide: bisacrylamide 19:1; Bio-Rad) containing 7 M urea. Radioactively labeled low-molecular-weight marker (Affymetrix, J76410) was used where indicated. The electrophoresis was performed in $1 \times$ TBE buffer (89 mM Tris, 89 mM boric acid, 2 mM EDTA). After running, the gels were fixed in fixing solution (40% methanol, 10% acetic acid, 5% glycerol) for 30 min at room temperature and subsequently dried, exposed to storage phosphor screen, and scanned by a Typhoon imager (GE Healthcare). The resulting images were analyzed with the ImageJ Software.

## 3. Results

### 3.1. Experimental assay

The aim of this study was to characterize tethering and bridging of long DNA molecules by the human (h) MRN and the yeast (y) MRX complexes, as well as their respective constituents (h/y)MR, NBS1 and Xrs2, on the single DNA molecule level and free in solution using nanofluidics. The study also aimed to further explore the capabilities of this method as a high throughput single molecule tool to characterize protein-DNA interactions. The assay, inspired by our previous study of CtIP/Sae2 [57], is shown in Fig. 1 for λ-DNA without protein added. The readout of the assay is based on the use of λ-phage DNA (λ-DNA) as a substrate, which - has 12 nt-long 5′-terminated complementary single-stranded overhangs that can hybridize both intra- and intermolecularly to form a circular or a concatemeric conformation, respectively (Fig. 1B) [56,57]. The 12 nt hybridized ends are sufficiently strong not to de-hybridize when introduced to a nanochannel, which allows any conformational change to happen in bulk prior to being recorded as single molecules in the channels. Circles and concatemers are the product of two different types of bridging processes. The main difference is that circle formation requires the ends of a single λ-DNA molecule being brought into proximity, while a concatemer is a bimolecular process where the ends of two separate DNA molecules meet. If a protein promotes the formation of circles this is most likely a process where the protein binds to multiple positions along the length of the DNA, creating a protein-protein bridge between these points, holding the DNA strands parallel to each other and bringing the ends in proximity and increasing the likelihood of them hybridizing [57]. The other option is an end-specific process that does not distinguish between circle- or concatemer formation, but rather specifically promotes the hybridization of the two overhangs. A large fraction of circles is thus a kinetic effect, where the circle formation, promoted by protein bridging, is so fast that the ends of different molecules do not have time to meet. To find which type of bridging process a protein of interest promoted we determined the average extension and the corresponding standard deviation ($STD_{Ext}$) of thousands of single DNA-protein complexes as described in the Methods section.

We demonstrate the principle of the experiment in Fig. 1 using λ-DNA without protein added. The scatter plot of extension vs. $STD_{Ext}$ (Fig. 1C) can be used to determine the relative abundance of each category. Without protein added, the largest cluster of molecules was full length, linear λ-DNA molecules (highlighted in yellow). Circular DNA molecules were rare for λ-DNA, but could be readily identified at an extension of approximately half of a full-length linear λ-DNA molecule [68] and a significantly smaller $STD_{Ext}$ (red) [68,69]. We also observed

λ-DNA molecules that were shorter than full length λ-DNA, but had a higher $STD_{Ext}$ than circularized λ-DNA (black). These molecules are either fragmented DNA molecules that lack at least one of the overhangs, and are hence not able to form circles, or circularized λ-DNA molecules that are in the process of unfolding from a circularized to a linear conformation (discussed further below). We finally observed a fraction of molecules that had a significantly larger extension than full length λ-DNA (blue). These are concatemers formed by spontaneous intermolecular hybridization of the overhangs, and they are also rare for λ-DNA without any proteins added. The relative abundance of each conformational population for bare λ-DNA can be found in Fig. 1D. In order to take into account that a concatemeric molecule that is > 2 monomers in length in fact is the result of more than one bridging event we calculated an "end-joining" (EJ) ratio (Methods). In short, the EJ-ratio weighs a circle as one bridging event and each concatemer based on the multiples of monomers within each concatemer. The EJ-ratio for λ-DNA is reported in Fig. 1E and is the likelihood of a molecule being part of a EJ-event. Associated to the EJ-ratio is "$P_{circ}$" and "$P_{conc}$". These numbers indicate the likelihood of an EJ-event being either formation of a circle or concatemer and are reported together with the EJ-ratio (Fig. 1E). For bare λ-DNA there is a 5% chance of random bridging and an almost equal likelihood of this bridging being circularization or concatemerization at the DNA concentration used.

### 3.2. MRN and MRX exhibit distinct DNA tethering capacities

Prior to the nanofluidic experiments, the DNA binding activities of the used proteins were characterized with EMSA (Fig. 2). The human proteins MRN, hMR and NBS1 all showed strong DNA binding activity that increased with increasing protein concentration (Fig. 2A). We observed that both yMR and MRX, could bind linearized plasmid DNA (~3 kb) (Fig. 2B). The DNA binding of yMR/MRX was enhanced in the presence of the non-hydrolysable ATP analogue, ATP-γ-S, which is in agreement with previous observations [70,71]. EMSA experiments with Xrs2 did also indicate a strong binding to DNA (Fig. 2C). In Fig. 2D–E representative and quantified results from an endonuclease assay is presented [. From these we can observe that the yeast proteins do not only bind to DNA but also show the expected endonucleolytic activity in the presence of Sae2.

In the single DNA molecule experiments in the nanofluidic setup, we observed a substantial difference in the histograms for both the extension and $STD_{Ext}$ for λ-DNA mixed with 60 nM MRN (Fig. 3A) or 60 nM MRX (Fig. 3B) compared to the control with only λ-DNA. For both MRN and MRX, and along both axes, there is a peak in the histogram at the position where circular molecules are expected to cluster, showing that both MRN and MRX promote intramolecular tethering of λ-DNA, which results in circularization of λ-DNA. Additionally, in both cases, a significant number of molecules with a longer extension than linear λ-DNA were observed, showing that both MRN and MRX also promote intermolecular bridging, also referred to as concatemerization (blue points in Fig. 3A–B). We next compared the concatemeric populations generated by MRN and MRX by estimating how many multiples of monomers that contribute to each concatemer. The result of this comparison is reported in Fig. 3C. There is a distinct difference in the concatemers formed by MRN and MRX. Whereas MRX promotes the formation of very long concatemers, MRN shows no concatemers longer than a multiple of three λ-DNA monomers.

Averaging data from at least three technical replicates provided a mean value of each conformational fraction at several protein concentrations for both MRN and MRX. The bars indicate the standard deviation of the mean value. Fig. 3D shows how the DNA bridging by MRN increased consistently with increasing protein concentration, both for circles and concatemers. The appearance of both circles and concatemers is strong evidence that MRN promotes hybridization of the 12-bp overhangs by bringing the λ-DNA ends close together. The fact that the concatemer fraction was substantially smaller than the fraction of
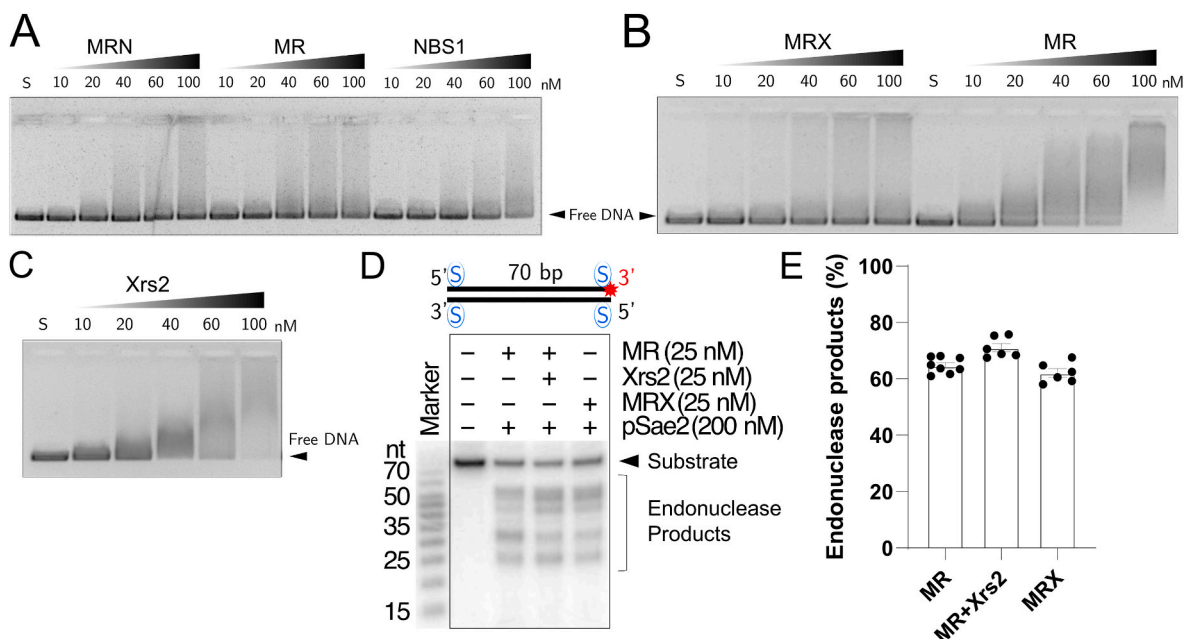
**Fig. 2. A)** Representative results from EMSA for increasing concentrations of MRN, hMR and NBS1 with 100 ng linearized pUC19 in Tris-OAc 25 mM, DTT 1 mM, EDTA 2 mM, BSA 50 μg/ml. **B)** Representative results from EMSA for increasing concentrations of MRX and yMR with 100 ng linearized pUC19 in Tris-OAc 25 mM, DTT 1 mM, MgOAc 2 mM, BSA 50 μg/ml and ATPγS 1 mM. **C)** Representative results from EMSA for increasing concentration of Xrs2 with 100 ng linearized pUC19 in Tris-OAc 25 mM, DTT 1 mM, EDTA 2 mM, BSA 50 μg/ml. **D)** Representative gel image from endonuclease experiments demonstrating the resection by MR + Xrs2 and MRX. **E)** Quantitation of endonuclease experiments in Fig. 2D.

circular molecules suggests that MRN primarily interacts with λ-DNA by bridging the molecule in an intramolecular manner that brings the two ends of one DNA molecule in close proximity, which increases the likelihood of hybridization. This is thus a kinetic effect where the intramolecular annealing of the overhangs is faster than the intermolecular bridging, an effect also observed in our previous study on CtIP [57]. Similarly, the number of bridging events by MRX increases with increasing protein concentration (Fig. 3E), but MRX did not show the same tendency of circularizing λ-DNA as MRN, but instead generated a larger fraction of concatemers. These observations suggest a slightly different interaction between MRX and λ-DNA compared to MRN, since circularization is not as efficient, potentially due to less efficient intramolecular DNA bridging.

The difference in DNA bridging between MRN and MRX is further accentuated by the EJ-ratio and $P_{circ}/P_{conc}$. From the EJ-ratio it is apparent that MRX is more efficient in bridging DNA than MRN (Fig. 3F–G). Comparing $P_{circ}/P_{conc}$ we can observe that MRN shows very small differences across conditions while MRX on the other hand shows a small increase in $P_{conc}$ with concentration together with a corresponding decrease in $P_{circ}$, pointing toward a concentration dependent shift in bridging activity.

To further investigate the differences between MRN and MRX, and confirm the binding of the proteins to DNA, we deposited the DNA-protein complexes on positively charged glass substrates. To localize the proteins on the DNA, a His-tag specific aptamer [65] was conjugated to QDOTs and added to the sample (see Methods). Control experiments demonstrated that the QDOTs only colocalized with DNA if proteins were bound to the DNA (Supplementary Figs. 2 and 4). For MRN we observed that a majority of the DNA-protein complexes were either in small stretched out groups with the protein bound in the junction between individual DNA molecules, or in small, compacted particles, which can be interpreted as single λ-DNA molecules bound by a cluster of proteins (Fig. 3H). The observations confirm the interpretation of the scatter plots that MRN tends to interact with λ-DNA in an intramolecular fashion. In stark contrast, MRX generated very large complexes when bound to λ-DNA, with signal from QDOTs colocalizing to the center of

the complex, indicating a large concentration of proteins in the center, which can be explained by oligomerization of yMR [52]. Since the nanochannel dimensions need to be sufficiently small to stretch the DNA, these large clusters did not enter the channels for the analysis above, which leads us to believe that the data captured in the nanofluidic devices might, for MRX, exclude some of the largest concatemers.

### 3.3. Neither human nor yeast MR show substantial bridging activity

To explore the differences between MRN and MRX further, and acknowledging previous evidence that MR is important for DNA tethering [38], we next investigated hMR and yMR. We first used protein concentrations (40–80 nM), which were comparable with those used in the experiments in Fig. 3. At these concentrations, the proteins promoted the formation of circles or concatemers to a much lower extent (Fig. 4A), compared to MRN/MRX (Fig. 3D–E). These data are in contrast with the EMSA experiments (Fig. 2B), where the same preparation of yMR showed a higher DNA binding activity compared to MRX, demonstrating that the formation of circles or concatemers in the nanofluidic setup is not a simple consequence of DNA binding.

A primary function of both MRN and MRX is to resect broken DNA ends as an initial step of HR [72]. While hMR needs the presence of NBS1 to be able to function fully as an endonuclease [25], yMR and MRX are comparably efficient in DNA end resection [29]. We used a nuclease assay to confirm the comparable nuclease activity of the yMR and MRX preparations used here (Fig. 2D–E). Hence, the observed differences in bridging activities between MR and MRX cannot be explained by an inactive preparation of yMR.

As previous studies have indicated, DNA bridging by MR is only stable at higher protein concentrations [38], possibly requiring MR oligomerization [52], we repeated the nanofluidic assay with hMR and yMR at increased protein concentrations. At ~5-fold higher protein concentrations we observed the formation of circles and concatemers to a much larger extent (Fig. 4B), but still lower than for MRN or MRX (Fig. 3D and E). Importantly, similarly to MRN/X, we observed a larger concatemeric fraction in experiments with yMR compared to hMR,
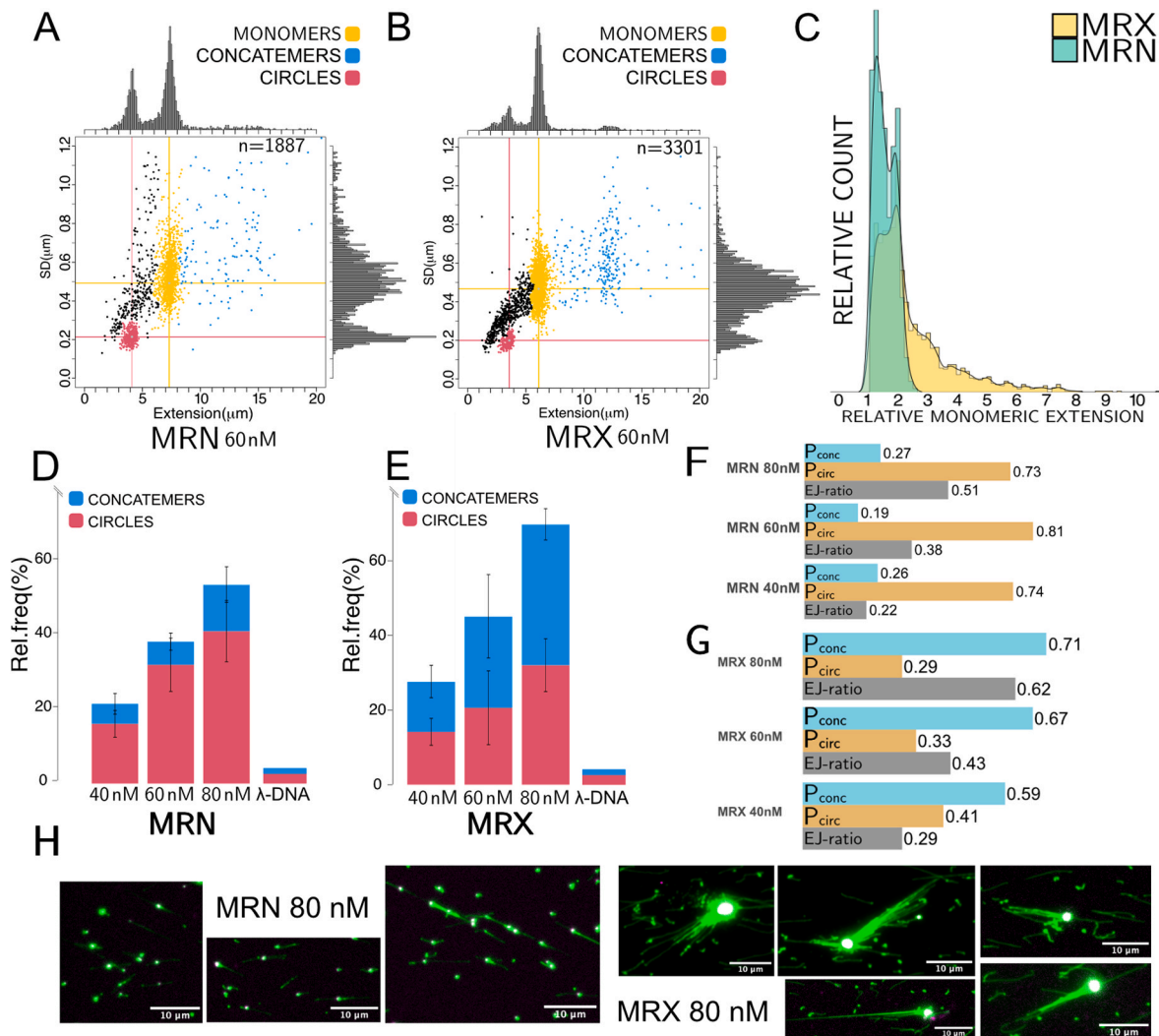
**Fig. 3. A)** DNA molecules imaged in the presence of 60 nM MRN. Scatterplot shows STD$_{Ext}$ of molecules against their extension. Red points indicate molecules classified as circles, yellow as the linear molecules and blue as concatemers. **B)** Same data for 60 nM MRX. **C)** The concatemeric population for MRN and MRX expressed in multiples of a linear λ-DNA molecule. **D)** Relative fraction of each population for increasing concentrations of MRN together with control data for λ-DNA alone. The data is based on 3 replicates and N = 6173, 6375 and 5213, respectively. **E)** Same data for MRX. N = 6429, 5377 and 3575, respectively **F)** "End-joining" ratio for MRN. A low ratio indicates a low number of "end-joining events" per observed monomer. A ratio > 1 indicates that there are more observed "end-joining events" than monomers. **G)** "end-joining" ratio for MRX. **H)** Representative images from protein λ-DNA complexes deposited on functionalized glass substrate with His-tag aptamer-conjugated QDOTS for protein localization. DNA is depicted in green and QDOT signal in magenta. (For interpretation of the references to color in this figure legend, the reader is referred to the Web version of this article.)

while hMR showed a larger fraction of circles relative to yMR. This suggests that neither NBS1 nor Xrs2 are required for the bridging, but that they contribute significantly to its effectiveness.

In order to confirm that the low bridging activity of h/yMR at lower concentrations was not due to low DNA binding, we again deposited the DNA-protein complexes on functionalized glass at a protein concentration of 80 nM, where very few circles and concatemers were observed in the nanofluidic experiments. A majority of the inspected molecules were single monomeric λ-DNA or small concatemers with indications of MR proteins bound at the ends (Fig. 4C). The samples differed in that yMR showed a lot of examples where the protein could be found along the length of the DNA whereas hMR included more examples of protein bound at the ends of the DNA or at the junction between molecules. We could find the h/yMR proteins on the DNA at low concentrations (Fig. 4C), showing that they are proficient in DNA binding, in agreement with the EMSA experiments (Fig. 2A–B). Despite their proficiency in DNA binding, we conclude that the MR complexes are notably less efficient in DNA bridging compared to MRN/X.

### 3.4. NBS1 and Xrs2 are important for the joining of DNA ends by MRN and MRX

We next explored if the significant difference in DNA bridging activity between MRN/X and h/yMR could be attributed to NBS1 and Xrs2 (Fig. 4D). We note from our EMSA results that both NBS1 and Xrs2 bind to DNA (Fig. 2A–C). The results from our nanofluidics setup indicate that both NBS1 and Xrs2 promote the hybridization of the overhangs of λ-DNA. The relative populations of circles and concatemers are comparable to h/yMR at similar concentrations, but not as high as for MRN and MRX. Interestingly, NBS1 showed a higher tendency to promote the formation of circularized λ-DNA molecules, whereas Xrs2 almost solely generated concatemers. This difference is further accentuated when also comparing the size of the concatemers, where concatemers generated by Xrs2 were significantly longer than concatemers observed in experiments with NBS1(Fig. 4E), just as the case for MRX in comparison to MRN (Fig. 3C).

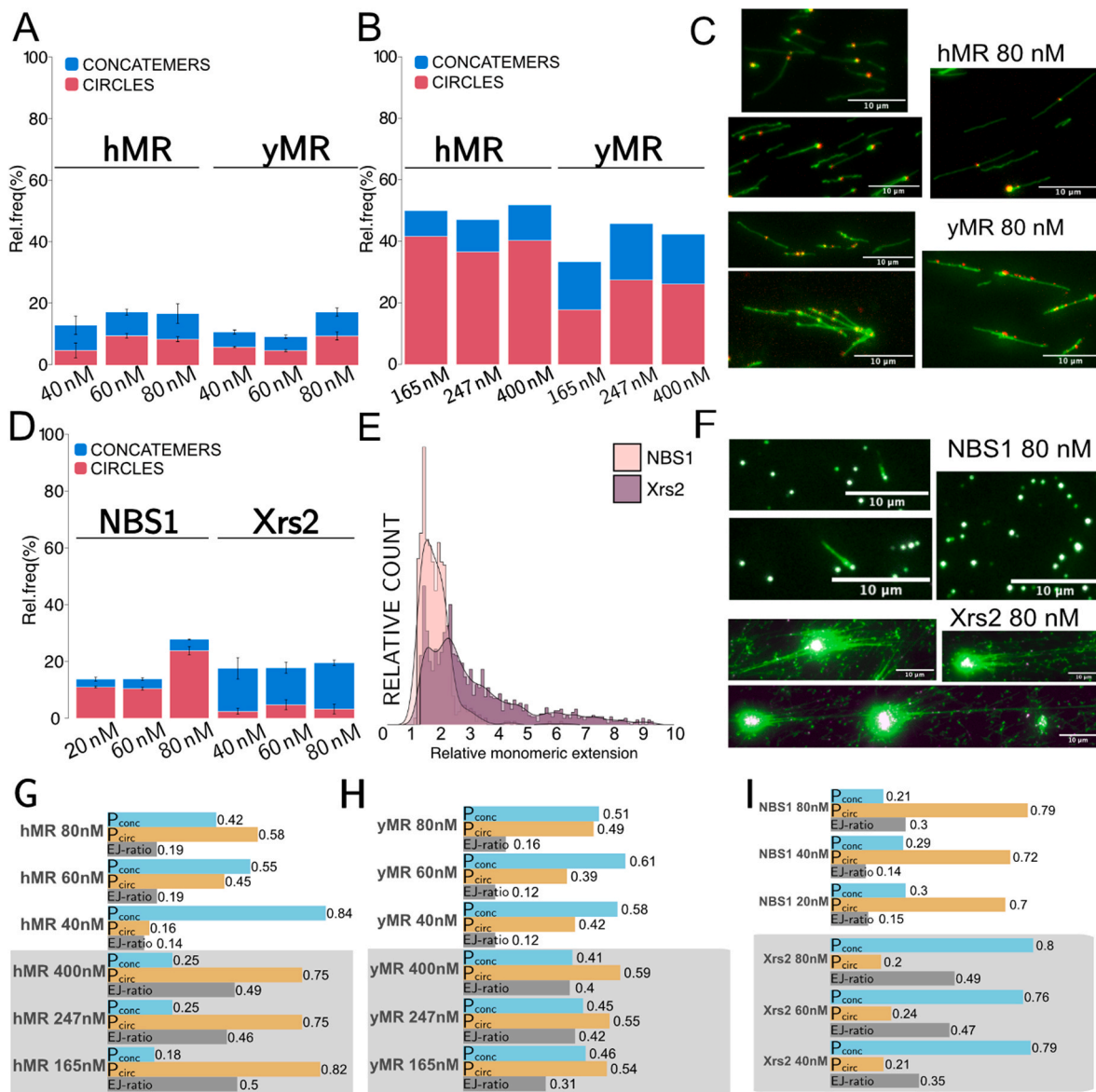It has previously been reported that Xrs2 has an intrinsic DNA

**Fig. 4.** **A)** Relative fractions of circularized and concatemeric λ-DNA in the presence of increasing, but comparable, concentrations of hMR (N = 2688, 2959, 5135) and yMR (N = 5609, 4889, 5660). For control data refer to Fig. 1C–D. **B)** Same type data for 5-fold higher concentrations of hMR(N = 3805, 4477, 2838) and yMR(N = 3019, 2433, 3182). For control data refer to Fig. 1C–D. **C)** Representative images of hMR and yMR bound to λ-DNA and deposited on functionalized glass substrates localized by His-tag aptamer conjugated QDOTs to visualize the binding sites of the proteins. **D)** Relative fractions of circularized and concatemeric λ-DNA in the presence of increasing, but comparable, concentrations of NBS1(N = 6705, 7268, 8407) and Xrs2(N = 2766, 3036, 2955). For control data refer to Fig. 1C–D. **E)** The concatemeric population for NBS1 and Xrs2 expressed in multiples of a linear λ-DNA molecule. **F)** λ-DNA bound by NBS1 or Xrs2 deposited on functionalized glass localized by His-tag aptamer conjugated QDOTs to visualize the binding sites of the proteins. **G)** "end-joining" ratio for hMR. A low ratio indicates a low number of "end-joing events" per observed monomer. A ratio > 1 indicates that there are more observed "end-joining events" than monomers. **H)** "end-joining" ratio for yMR. **I)** "end-joining" ratio for NBS1 and Xrs2.

binding ability, which helps guiding MRX to DNA ends [53]. This ability could be in agreement with the very specific bridging activity of Xrs2 detected in our assay, but no such observations have been reported for NBS1. Experiments with Xrs2 and aptamer-conjugated QDOTs on glass slides show very large DNA complexes that consist of a large amount of circularized and/or concatemeric λ-DNA with a large core of proteins (Fig. 4F), just as for MRX. Complexes of this size are impossible to properly introduce into the nanofluidic channels, which would suggest that the ability of Xrs2 to form concatemers is underestimated in Fig. 4D since a lot of DNA molecules appears to be included in larger structures. For NBS1 bound to DNA we found very few large DNA clusters on the glass slides (Fig. 4F). A majority of the observed DNA-protein complexes were comparably small and condensed DNA molecules, which would be

in line with the results from the nanofluidic assay. This is also aligned with what we observed for MRN on the glass slides (Fig. 3F).

We next determined the EJ-ratio for both yMR, hMR, NBS1 and Xrs2. For hMR there is a more than two-fold higher EJ-ratio for the "high" concentration experiments compared to the "low" ones (Fig. 4G). A second significant observation is the difference in $P_{circ}/P_{conc}$ between the "low" and "high" concentrations where the "low" range shows a concentration dependent shift from concatemer formation to circle formation. This supports the idea that circle formation is due to intra-molecular bridging that is increased at increased protein concentrations. This conversion seems to have been completed in the "high" concentration range where there is little to no difference between the conditions.

We observe a similar relation between the "low" and "high" concentration conditions regarding the EJ-ratio for yMR as for hMR (Fig. 4H), although, over all, slightly lower for yMR. This would not necessarily be expected looking to the bridging response since the concatemeric fraction, which contributes more to the EJ-ratio than circles, for "high" yMR is slightly larger compared to for hMR, Fig. 4B. While hMR showed a conversion in bridging type between the "low" and "high" concentrations, yMR does not show such a trend and we observe no significant difference in $P_{circ}/P_{conc}$ between concentrations for yMR.

$P_{circ}$ for NBS1 is consistently high for all conditions, suggesting that the end-joining events occurring are mostly circularization (Fig. 4I). This is confirmed in the density plot in Fig. 4E where the length of the concatemers does not extend beyond 3-mers. Interestingly, Xrs2 shows a different trend despite the total number of circles and concatemers being similar. From the EJ-ratio we can see that Xrs2 has an almost 2-fold higher apparent EJ efficiency compared to NBS1, which increases with concentration (Fig. 4I). This is further accentuated by the length of the concatemers that extends up to at least 10-mers in length. Interestingly, the likelihood of concatemer formation does not increase with Xrs2 concentration.

The results for NBS1 and Xrs2 demonstrate that they both play an integral part in the DNA bridging by the full MRN and MRX complexes, respectively, as well as have a distinct DNA binding capacity on their own. It is interesting to notice that neither NBS1, Xrs2 nor h/yMR show the same degree of bridging as the full MRN and MRX complexes. This suggests that there is an apparent synergistic effect when NBS1 and Xrs2 bind to their respective MR partners within the MRN/X complexes, leading to enhanced DNA bridging. Xrs2 makes an interesting exception to this and shows an exceptionally high EJ ratio compared to its degree of bridging, which speaks towards a tendency to generate very long but few concatemers, something that is further validated with direct visualization in glass slide experiments.

### 3.5. MRN and MRX form local compactions on circular DNA

In addition to providing the extension and standard deviation for thousands of molecules, we also obtained images of the DNA-protein complexes in the nanofluidic channels. These images can for example
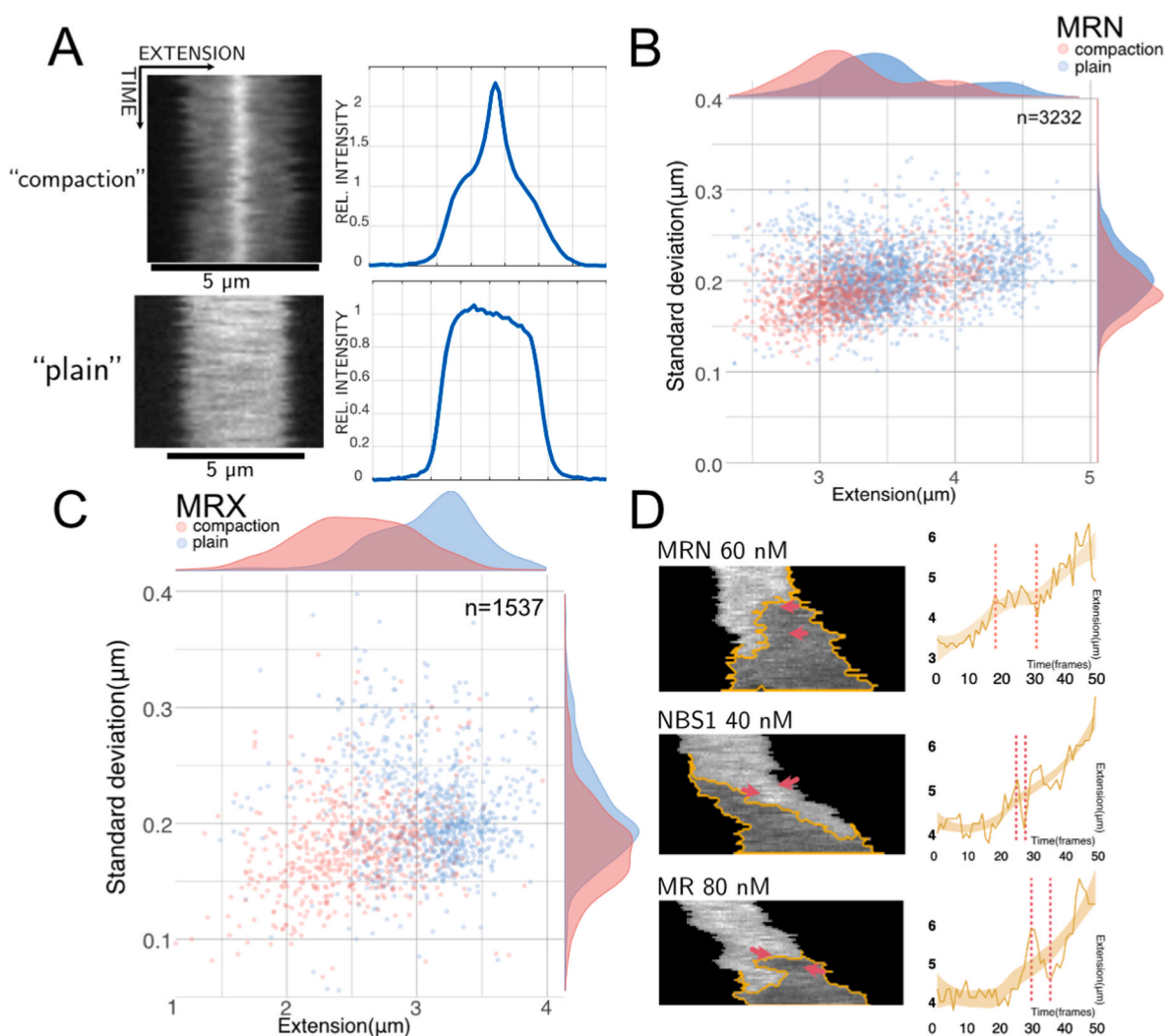


**Fig. 5. A)** Representative kymographs from each subcategory identified within the circular fraction of MRN and MRX data. "Compaction" refers to molecules with a local increase in intensity and "plain" to molecules with an evenly distributed intensity profile. **B)** Circular molecules formed in the presence of MRN. Scatterplot showing the $STD_{Ext}$ of molecules against their extension with the distribution of each category along the axis. Each individual molecule was inspected and categorized according to A). **C)** Circular molecules formed in the presence of MRX. Scatterplot showing the $STD_{Ext}$ of molecules against their extension with the distribution of each category along the axis. **D)** Representative kymographs of λ-DNA, circularized by MRN, MR or NBS1, that unfolded during imaging. Each kymograph is supplemented with a graph showing the extension increase with time, as the molecule unfolds. Red arrows and dotted lines highlight different dynamic events where the unfolding process is hindered due to protein binding. Kymographs and extension graphs with additional examples can be found in Supplementary Fig. 5. (For interpretation of the references to color in this figure legend, the reader is referred to the Web version of this article.)

reveal information on the local density of DNA along the DNA contour [73]. To further define the differences between the DNA bridging of MRN and MRX, we investigated how the intensity varied along each individual molecule, both for the circular and linear DNA-protein complexes. We identified two major subpopulations, molecules that had a local peak in emission intensity ("compaction" in Fig. 5A) and, secondly, molecules that had an even fluorescence signal along the contour ("plain" in Fig. 5A). We previously reported similar observations of a higher local concentration for CtIP bound to circularized λ-DNA that was interpreted as a local protein accumulation, causing the DNA to locally condense [57]. The increase in the fluorescence emission suggests that both MRN and MRX change the physical properties of DNA to allow local compaction of the DNA in a way that was not observed for DNA without protein added [70]. Local compactions were much more common for the circular populations for both MRN (31%) and MRX (40%) than the linear (5% and 1%, respectively), so we will focus solely on discussing the circular fraction further. In the representative example of a molecule with a compaction shown in Fig. 5A, the compaction is located in the center of the DNA molecule, although we observed many examples with the compaction offset to one side or the other. There are also examples where the compaction seems to move along the DNA during the duration of imaging. This can most likely be explained by the DNA molecule rotating rather than the compaction traveling along the DNA, although it cannot be fully excluded.

Fig. 5B–C show scatter plots of the circular fractions according to the categories in Fig. 5A. The plots reveal that the local compactions on circular λ-DNA molecules shorten the observed extension significantly. In the presence of high concentrations of hMR (165–400 nM), roughly 13% of the circular molecules had local compactions, whereas 9% of the molecules had a compaction for yMR. In either case, the number of compactions was significantly lower compared to MRN and MRX, indicating that the full complex is necessary for these compactions to be very prevalent. Very few local compactions were observed for NBS1 or Xrs2 alone (<1%).

### 3.6. Unfolding of circularized molecules provides qualitative evidence of DNA tethering

As mentioned above, there is a fraction of molecules with high $STD_{Ext}$ above the cluster of circles and left to the cluster of linear molecules in Fig. 3A–B. Some of these molecules are circles that have started to unfold during imaging due to the formation of a DSB caused by fluorophore mediated photocleavage by YOYO-1. In previous studies of bare unfolding circles, it was found that the unfolding of a circular DNA molecule is a continuous process [68,74]. Another study found that circularized λ-DNA in the presence of T4 Ligase, both with and without ATP, unfolded slower than bare λ-DNA [75], suggesting that the protein bridges the parallel unfolding DNA strands. Fig. 5D shows representative examples of unfolding circular DNA-protein complexes for each of the human proteins MRN, MR and NBS1, together with a corresponding graph showing the increase in extension over time (additional examples in Supplementary Fig. 5). The jagged yellow line, which is the extension per frame, plateaus on several occasions in all kymographs. This "non-continuous" unfolding of λ-DNA only occurs in the presence of protein and can be explained by bridging of distant DNA fragments by the protein. The binding is seemingly transient in the sense that the force of the unfolding molecule is greater than the proteins' ability to retain the bridging and eventually the unfolding process continues to finally yield the linear configuration. We found multiple examples of this behavior for all human proteins, MRN, MR and NBS1, but few to none for the yeast proteins, with an exception for very high concentrations of yMR. This agrees with our observation that the human proteins bridge DNA intramolecularly to a higher degree. A protein that binds very specifically to the ends, like Xrs2, will be less likely to grab on to the opposing strand of the unfolding molecule. A second, contributing factor is the lower number of circles for the yeast proteins, making it less likely

to catch these unfolding while imaging.

## 4. Discussion

The main goal of this study was to study the role of MRN and MRX, and their subcomponents, in organizing DNA at DSBs and to better understand how nanofluidic channels can be used a tool for studies of such protein-DNA interactions. The main asset of the nanofluidics technique used here is the possibility to investigate DNA bridging and interactions with DNA ends, which have to some extent been overlooked in previous single molecule studies, due to difficulties in observing and analyzing bridging of DNA substrates with free DNA ends. Since the DNA molecules studied are free in solution, it is possible to study both intra- and intermolecular bridging as well as interactions between DNA ends. We have made several important observations that highlight the functionalities of the different components of MRN and MRX in their ability to tether and bridge DNA.

### 4.1. The nanofluidic assay

The employed nanofluidic assay used the formation of circles and concatemers of λ-DNA upon hybridization of the 12 nt-long complementary overhangs as a readout. Importantly, while both circularization and concatemerization depend on the hybridization of the overhangs, they are not identical. To understand how these two different events can be used to assess DNA bridging by a protein one needs to consider in what manner the DNA needs to be coerced in order for either type of conformational change to occur. Concatemer formation is an intermolecular process, where the ends of two different DNA molecules are hybridized. This process is mainly governed by end-specific interactions that promote, and potentially stabilize, the hybridization of DNA ends. An important factor to consider here is that intermolecular bridging is a diffusion dependent process and thus depends on the total concentration of DNA ends in the solution [57] as well as the propensity of the ends to hybridize. This means that an increase in the formation of concatemers entails a process that increases the access to the DNA ends, potentially by promoting hybridization of the overhangs. Translated to a biologically relevant situation, an example of a process within DNA repair that resembles the formation of concatemers would be the synapses that are formed when a DSB is repaired by NHEJ. In these situations, the ends are tethered by a protein-protein bridge in the same plane prior to ligation.

Circularization, on the other hand, is an intramolecular process that also can be promoted by end-specific interactions, but more importantly, by other processes that bring the two ends of the same single DNA molecule to come in close vicinity which increases the likelihood of them hybridizing. This entails that circularization of a DNA molecule is much more likely if a protein can bind and bridge the DNA along the length of the molecule rather than solely on the ends. A bridge between two arbitrary points on a DNA molecule forces the molecule to fold onto itself, bringing the ends in proximity and thus increasing the likelihood of hybridization. Together with protein-protein interactions bringing the ends in proximity there is also a possibility of contributions stemming from changes to the physical properties of the DNA. If a protein-DNA interaction decreases the self-avoidance of the DNA substrate this allows the molecule to bundle up closer to itself which in turn decreases the hydrodynamic radius of the molecule and with that the distance between the ends. The process that leads to circularization can be compared to when two distant parts of DNA are brought together and held together, but on parallel planes. This could for example be situations like an enhancer-promoter interaction or when a sister chromatid is tethered at a DSB for subsequent strand invasion and HR mediated repair.

It is important to realize that intramolecular and intermolecular bridging are competing processes and that the introduction of proteins is essentially changing the kinetics of these processes. While we observed very little spontaneous bridging in our control the few examples

recorded showed a next to equal likelihood of molecules being involved in circularization or bimolecular events. What the assay allows us to observe is how a protein of interest changes the relation between these two competing processes. With this in mind it is important to realize that neither circularization nor concatemerization are equivalent to biological processes per se, but rather a readout that indicates DNA bridging and which type of process that lies behind it.

### 4.2. The interaction between MRX and long DNA is heavily dependent on Xrs2

A key conclusion of our experiments is that Xrs2 strongly contributes to the DNA bridging activity of the MRX complex. Xrs2 carries a nuclear localization signal (NLS), and hence it is required for all cellular functions of the MRX complex. The nuclear import function of Xrs2 can however be bypassed by placing the NLS on Mre11. Such experiments with Mre11-NLS revealed a non-equal contribution of Xrs2 to the cellular DSB response [29,30]. An important observation is that Xrs2 is essential for the promotion of NHEJ and Tel1 activation, while it is largely dispensable for DNA end resection [76]. The contribution of Xrs2 to NHEJ was thought to be explained by the specific interaction between Xrs2 and Lif1, a component of the Dnl4-Lif1 ligase complex at the core of the NHEJ process [31]. The data presented here suggest that Xrs2 may promote NHEJ by stimulating the synapsis catalyzed by the MR complex.

The main difference observed between MRX and MRN is that for MRX fewer circles and more concatemers were formed. Additionally, the EJ-ratio suggests that MRX bridges DNA slightly more efficiently than MRN and does so by generating more and more concatemers. This suggests that MRX acts in a more end-specific manner that promotes bimolecular hybridization. Just as for the human complex, where MRN showed significantly higher DNA bridging than hMR, Xrs2 appeared to be crucial for this activity in yeast, since much higher concentrations of yMR were needed for to observe the same activity compared to MRX. Interestingly, Xrs2 also catalyzes the formation of concatemers on its own, although not to the same extent as MRX. Although, when looking to the EJ-ratio of Xrs2 it seems to be more efficient than the bridging response would first suggest. The fact that there is no discernible increase in concatemer formation with increasing concentrations, but an increase in EJ-ratio suggests that Xrs2 instead of making more concatemers, makes them longer since long concatemers contribute significantly to the number of EJ-events, but make little difference in the fractional populations. An interesting difference between MRX and Xrs2 is the fraction of circles formed by MRX. This suggests that the DNA bridging ability of MRX is an additive effect of Xrs2, since Xrs2 cannot form the intramolecular bridges, but MR and MRX can. TEM imaging of equivalent levels of MR have shown that MR loops DNA, but has a limited ability to bind at the ends [52]. The role of Xrs2 in DNA bridging is further elucidated by observations from DNA-protein complexes deposited on glass slides where very large DNA complexes could be observed in presence of MRX and Xrs2 but not MR. The complexes appear to have a lot of proteins localized to the center, indicating that the proteins create a large network of interactions with both DNA and protein interfaces. This would be in line with the observation of Xrs2 making longer concatemers rather than more with increasing concentrations, suggesting that protein-protein interactions between Xrs2 might have an enhancing effect on DNA binding. Interestingly, these observations are in stark contrast to the endonucleolytic activity, where the *in vitro* activity is identical for MR and MRX, and Xrs2 hence is redundant [19]. The fact that MR and MRX have a very similar nucleolytic activity, but differ distinctly in their bridging of DNA, points towards the importance of Xrs2 in MRX for this ability. Since the role as a nuclease is strongly connected to the HR pathway, this highlights the significant role of Xrs2 in the involvement of MRX in NHEJ. While NBS1 has an apparent role of stabilizing the MRE11 dimer and the MR complex, Xrs2's contribution is seemingly larger.

### 4.3. MR(N) bridges DNA more effectively in the presence of NBS1

The most important observation for MRN was that its DNA bridging capability was enhanced by NBS1. We observed a high degree of circularization and a low fraction of concatemers, suggesting that MRN bridges DNA regions intramolecularly. The ability of MRN to bridge DNA in our assay was largely stimulated by NBS1, since much higher concentrations were needed to reach the same level of DNA bridging with hMR compared to MRN. Furthermore, NBS1 on its own also promoted DNA bridging but to a significantly lower extent. Importantly, a large fraction of the bridged DNA complexes formed by NBS1, just as for MRN, was circles. Since intra- and intermolecular bridging are competing processes we cannot exclude that the human proteins, which show a higher degree of intramolecular hybridization, would have the same activity as the corresponding yeast proteins, if circularization was not possible.

It has been shown that MRN tethers DNA by MRE11 binding to the DNA backbone and the 'coiled-coils' of RAD50 connecting adjacent MRN complexes [28,50]. Additionally, a recent study of the MRN structure showed that NBS1 stabilizes the MRE11 dimer and that the ends of the 'coiled-coils' of RAD50 enable multiple MRN assemblies [46]. Such stabilization might help explain the efficient DNA tethering ability of MRN. The fact that NBS1 is indispensable for HR but does not affect NHEJ activity [34] is in line with MRN bridging DNA in a primarily intramolecular fashion, since this resembles a situation where two sister chromatids are held in proximity for subsequent HR, rather than a synapsis-like tethering that is needed for NHEJ. Experiments with protein-DNA complexes deposited on functionalized glass coverslips support this interpretation where we observed that both MRN and NBS1 generate small complexes with tightly packed DNA, whereas MR instead showed more examples of stretched DNA with protein bound along its length. These observations highlight the importance of NBS1 for the full function of the MRN complex and strengthens the evidence for an additional, structurally stabilizing, function of NBS1 besides the already established functions [23,25,59,77,78].

Direct, qualitative evidence of DNA bridging was observed in kymographs of circular DNA molecules that were unfolding during imaging. Without proteins present, the molecules unfold to the linear form in a continuous fashion. With proteins present, the unfolding is interrupted and happens in bursts, which we interpret as the DNA getting "captured" while unfolding. This can be explained by the protein holding the two overlapping strands together. This bridging eventually gets loose when the protein no longer holds on to both strands, and unfolding proceeds. This phenomenon was much less observed for the yeast proteins, in line with less efficient intramolecular DNA bridging.

#### 4.3.1. Localized compactions provide evidence for DNA bridging

For the molecules that are circularized by MRN or MRX, we, in many cases, observed a region of high local DNA density in kymographs, in particular for the circularized molecules. This accumulation is similar to what was observed for CtIP [57], but not for other DNA-binding proteins involved in DSB repair, such as Rad51 [79]. In our study of CtIP we proposed that these local DNA compactions are promoted by the binding of CtIP, and both MRN and MRX seem to have a similar effect. Interestingly we do not observe these compactions in the linear fraction for either of MRN or MRX. They are thus most likely formed where the protein bridges the DNA strands and brings them into close proximity.

### 5. Conclusions

To conclude, we have shown that nanofluidic channels can be a powerful tool in the investigation of DNA binding proteins and their interaction with long DNA substrates. In particular, we have elucidated the distinct ways in which MRN and MRX tether long DNA and promote the subsequent hybridization of their ends. Significantly, we found that both NBS1 and Xrs2 play a crucial role in the bridging of long DNA

molecules and that Xrs2 has a strong individual tethering ability, results that are in line with previous reports which have pointed towards the importance of NBS1 in HR [34] and Xrs2 in NHEJ [29,30].

## Funding

This project was funded by the Swedish Research Council (2020–03400 to FW), Stiftelsen Olle Engqvist Byggmästare (to FW), the European Research Council in the form of a ERC consolidator grants to FW (no. 866238). The Swiss National Science Foundation (SNSF) (Grants 310030_207588 and 310030_205199) and the European Research Council (ERC) (Grant 101018257) support the research in the Cejka laboratory.

## CRediT authorship contribution statement

**Carl Möller:** Writing – original draft, Methodology, Formal analysis, Data curation. **Rajhans Sharma:** Writing – review & editing, Investigation, Formal analysis. **Robin Öz:** Investigation, Formal analysis, Data curation. **Giordano Reginato:** Resources, Investigation. **Elda Cannavo:** Resources, Investigation. **Ilaria Ceppi:** Resources, Investigation. **K.K. Sriram:** Writing – review & editing, Resources. **Petr Cejka:** Writing – review & editing, Supervision, Project administration, Funding acquisition, Conceptualization. **Fredrik Westerlund:** Writing – original draft, Supervision, Project administration, Funding acquisition, Conceptualization.

## Declaration of competing interest

The authors declare that they have no known competing financial interests or personal relationships that could have appeared to influence the work reported in this paper.

## Acknowledgements

We acknowledge the group of Prof. Tobias Ambjörnsson at Lund University for developing the software for analyzing the nanofluidics experiments. Nanofluidic devices were fabricated at MyFab Chalmers cleanroom facility. A special thank you to Dr. My Nyblom for contributing to illustrations and to Dr. Albertas Dvirnas for valuable technical support on data analysis.

## Appendix A. Supplementary data

Supplementary data to this article can be found online at https://doi.org/10.1016/j.bbrc.2023.149464.

## References

[1] M.K. Zeman, K.A. Cimprich, Causes and consequences of replication stress, Nat. Cell Biol. 16 (2014) 2–9.

[2] M.E. Lomax, L.K. Folkes, P. O'Neill, Biological consequences of Radiation-induced DNA damage: relevance to radiotherapy, Clin. Oncol. 25 (2013) 578–585.

[3] A. Syed, J.A. Tainer, The MRE11-RAD50-NBS1 complex conducts the orchestration of damage signaling and outcomes to stress in DNA replication and repair, Annu. Rev. Biochem. 87 (2018) 263–294.

[4] J. Lafrance-Vanasse, G.J. Williams, J.A. Tainer, Envisioning the dynamics and flexibility of Mre11-Rad50-Nbs1 complex to decipher its roles in DNA replication and repair, Prog. Biophys. Mol. Biol. 117 (2015) 182–193.

[5] G. Reginato, P. Cejka, The MRE11 complex: a versatile toolkit for the repair of broken DNA, DNA Repair 91–92 (2020) 102869.

[6] A.S. Kawale, P. Sung, Mechanism and significance of chromosome damage repair by homologous recombination, Essays Biochem. 64 (2020) 779–790.

[7] C.B. Schiller, et al., Structure of Mre11–Nbs1 complex yields insights into ataxia-telangiectasia–like disease mutations and DNA damage signaling, Nat. Struct. Mol. Biol. 19 (2012) 693–700.

[8] D. Nakada, ATM-related Tel1 associates with double-strand breaks through an Xrs2-dependent mechanism, Genes Dev. 17 (2003) 1957–1962.

[9] D.A. Bressan, H.A. Olivares, B.E. Nelms, J.H. Petrini, Alteration of N-terminal phosphoesterase signature motifs inactivates Saccharomyces cerevisiae Mre11, Genetics 150 (1998) 591–600.

[10] M. Furuse, et al., Distinct roles of two separable in vitro activities of yeast Mre11 in mitotic and meiotic recombination, EMBO J. 17 (1998) 6412–6425.

[11] K.M. Trujillo, S.-S.F. Yuan, E.Y.-H.P. Lee, P. Sung, Nuclease activities in a complex of human recombination and DNA repair factors Rad50, Mre11, and p95, J. Biol. Chem. 273 (1998) 21447–21450.

[12] T. Usui, et al., Complex Formation and functional versatility of Mre11 of budding yeast in recombination, Cell 95 (1998) 705–716.

[13] S. Moreau, J.R. Ferguson, L.S. Symington, The nuclease activity of Mre11 is required for meiosis but not for mating type switching, end joining, or telomere maintenance, Mol. Cell Biol. 19 (1999) 556–566.

[14] T.T. Paull, M. Gellert, The 3′ to 5′ exonuclease activity of Mre11 facilitates repair of DNA double-strand breaks, Mol Cell 1 (1998) 969–979.

[15] K.-P. Hopfner, et al., The Rad50 zinc-hook is a structure joining Mre11 complexes in DNA recombination and repair, Nature 418 (2002) 562–566.

[16] K. Lammens, et al., The mre11:rad50 structure shows an ATP-dependent molecular clamp in DNA double-strand break repair, Cell 145 (2011) 54–66.

[17] Y. Liu, et al., ATP-dependent DNA binding, unwinding, and resection by the Mre11/Rad50 complex, EMBO J. 35 (2016) 743–758.

[18] F.U. Seifert, K. Lammens, B. Kessler, K. Hopfner, Structural mechanism of ATP-dependent DNA binding and DNA end bridging by eukaryotic Rad50, EMBO J. 35 (2016) 759–772.

[19] E. Cannavo, G. Reginato, P. Cejka, Stepwise 5′ DNA end-specific resection of DNA breaks by the Mre11-Rad50-Xrs2 and Sae2 nuclease ensemble, Proc. Natl. Acad. Sci. USA 116 (2019) 5505–5513.

[20] E.P. Mimitou, L.S. Symington, Sae2, Exo1 and Sgs1 collaborate in DNA double-strand break processing, Nature 455 (2008) 770–774.

[21] G. Reginato, E. Cannavo, P. Cejka, Physiological protein blocks direct the Mre11–Rad50–Xrs2 and Sae2 nuclease complex to initiate DNA end resection, Genes Dev. 31 (2017) 2325–2330.

[22] A. Shibata, et al., DNA double-strand break repair pathway choice is directed by distinct MRE11 nuclease activities, Mol Cell 53 (2014) 7–18.

[23] H. Wang, et al., The interaction of CtIP and Nbs1 connects CDK and ATM to regulate HR–mediated double-strand break repair, PLoS Genet. 9 (2013) e1003277.

[24] K. Matsuzaki, A. Shinohara, M. Shinohara, Forkhead-associated domain of yeast Xrs2, a homolog of human Nbs1, promotes nonhomologous end joining through interaction with a ligase IV partner protein, Lif1, Genetics 179 (2008) 213–225.

[25] R. Anand, et al., NBS1 promotes the endonuclease activity of the MRE11-RAD50 complex by sensing CtIP phosphorylation, EMBO J. 38 (2019).

[26] J. Oh, A. Al-Zain, E. Cannavo, P. Cejka, L.S. Symington, Xrs2 dependent and independent functions of the mre11-rad50 complex, Mol Cell 64 (2016) 405–415.

[27] Y. Tsukamoto, C. Mitsuoka, M. Terasawa, H. Ogawa, T. Ogawa, Xrs2p regulates Mre11p translocation to the nucleus and plays a role in telomere elongation and meiotic recombination, Mol. Biol. Cell 16 (2005) 597–608.

[28] R. Tisi, J. Vertemara, G. Zampella, M.P. Longhese, Functional and structural insights into the MRX/MRN complex, a key player in recognition and repair of DNA double-strand breaks, Comput. Struct. Biotechnol. J. 18 (2020) 1137–1152.

[29] J. Oh, A. Al-Zain, E. Cannavo, P. Cejka, L.S. Symington, Xrs2 dependent and independent functions of the mre11-rad50 complex, Mol Cell 64 (2016) 405–415.

[30] J. Oh, S.J. Lee, R. Rothstein, L.S. Symington, Xrs2 and Tel1 independently contribute to MR-mediated DNA tethering and replisome stability, Cell Rep. 25 (2018) 1681–1692.e4.

[31] L. Chen, K. Trujillo, W. Ramos, P. Sung, A.E. Tomkinson, Promotion of Dnl4-catalyzed DNA end-joining by the rad50/mre11/xrs2 and Hdf1/Hdf2 complexes, Mol Cell 8 (2001) 1105–1115.

[32] T.T. Paull, M. Gellert, A Mechanistic Basis for Mre11-Directed DNA Joining at Microhomologies, 2000. www.pnas.orgcgidoi10.1073pnas.110144297.

[33] D. Udayakumar, C.L. Bladen, F.Z. Hudson, W.S. Dynan, Distinct pathways of nonhomologous end joining that are Differentially regulated by DNA-dependent protein kinase-mediated phosphorylation, J. Biol. Chem. 278 (2003) 41631–41635.

[34] H. Tauchi, et al., Nbs1 is essential for DNA repair by homologous recombination in higher vertebrate cells, Nature 420 (2002) 93–98.

[35] J.H. Kim, et al., The mre11-Nbs1 interface is essential for viability and tumor suppression, Cell Rep. 18 (2017) 496–507.

[36] M. Kong, E.C. Greene, Mechanistic insights from single-molecule studies of repair of double strand breaks, Front. Cell Dev. Biol. 9 (2021) 3265.

[37] K. Kaniecki, L. De Tullio, E.C. Greene, A change of view: homologous recombination at single-molecule resolution, Nat. Rev. Genet. 19 (2018) 191–207.

[38] F. Moreno-Herrero, et al., Mesoscale conformational changes in the DNA-repair complex Rad50/Mre11/Nbs1 upon binding DNA, Nature 437 (7057) (2005) 440–443, 2005 437.

[39] H. Tatebe, et al., Rad50 zinc hook functions as a constitutive dimerization module interchangeable with SMC hinge, Nat. Commun. 11 (2020) 1–11.

[40] E. Zabolotnaya, et al., Modes of action of the archaeal Mre11/Rad50 DNA-repair complex revealed by fast-scan atomic force microscopy, Proc. Natl. Acad. Sci. U. S. A. 117 (2020) 14936–14947.

[41] L.R. Myler, et al., Single-molecule imaging reveals how mre11-rad50-Nbs1 initiates DNA break repair, Mol Cell 67 (2017) 891–898.e4.

[42] R.A. Deshpande, et al., DNA-dependent protein kinase promotes DNA end processing by MRN and CtIP, Sci. Adv. 6 (2020) eaay0922.

[43] M. De Jager, et al., Human rad50/mre11 is a flexible complex that can tether DNA ends, Mol Cell 8 (2001) 1129–1135.

[44] E. Kinoshita, S. Van Rossum-Fikkert, H. Sanchez, A. Kertokalio, C. Wyman, Human RAD50 makes a functional DNA-binding complex, Biochimie 113 (2015) 47–53.

[45] E. Van der linden, H. Sanchez, E. Kinoshita, R. Kanaar, C. Wyman, RAD50 and NBS1 form a stable complex functional in DNA binding and tethering, Nucleic Acids Res. 37 (2009) 1580–1588.

[46] M. Rotheneder, et al., Cryo-EM structure of the Mre11-Rad50-Nbs1 complex reveals the molecular mechanism of scaffolding functions, Mol Cell (2022), https://doi.org/10.1016/j.molcel.2022.12.003.

[47] C. Möckel, K. Lammens, A. Schele, K.-P. Hopfner, ATP driven structural changes of the bacterial Mre11:Rad50 catalytic head complex, Nucleic Acids Res. 40 (2012) 914–927.

[48] E. Kinoshita, S. van Rossum-Fikkert, H. Sanchez, A. Kertokalio, C. Wyman, Human RAD50 makes a functional DNA-binding complex, Biochimie 113 (2015) 47–53.

[49] S. Sung, et al., DNA end recognition by the Mre11 nuclease dimer: insights into resection and repair of damaged DNA, EMBO J. 33 (2014) 2422–2435.

[50] K.P. Hopfner, et al., The Rad50 zinc-hook is a structure joining Mre11 complexes in DNA recombination and repair, Nature 418 (6897) (2002) 562–566, 2002 418.

[51] E. Zabolotnaya, et al., Modes of action of the archaeal Mre11/Rad50 DNA-repair complex revealed by fast-scan atomic force microscopy, Proc. Natl. Acad. Sci. U. S. A. 117 (2020) 14936–14947.

[52] V.M. Kissling, et al., Mre11-Rad50 oligomerization promotes DNA double-strand break repair, Nat. Commun. 13 (1) (2022) 1–16, 2022 13.

[53] K.M. Trujillo, et al., Yeast xrs2 binds DNA and helps target rad50 and mre11 to DNA ends, J. Biol. Chem. 278 (2003) 48957–48964.

[54] K. Frykholm, L.K. Nyberg, F. Westerlund, Exploring DNA–protein interactions on the single DNA molecule level using nanofluidic tools, Integr. Biol. 9 (2017) 650–661.

[55] K. Frykholm, V. Müller, K.D. Dorfman, F. Westerlund, DNA in nanochannels: theory and applications, Q. Rev. Biophys. (2022), https://doi.org/10.1017/S0033583522000117.

[56] R. Öz, et al., Dynamics of Ku and bacterial non-homologous end-joining characterized using single DNA molecule analysis, Nucleic Acids Res. 49 (2021) 2629–2641.

[57] R. Öz, et al., Phosphorylated CtIP bridges DNA to promote annealing of broken ends, Proc. Natl. Acad. Sci. U. S. A. 117 (2020) 21403–21412.

[58] E. Cannavo, P. Cejka, S.C. Kowalczykowski, Relationship of DNA degradation by Saccharomyces cerevisiae Exonuclease 1 and its stimulation by RPA and Mre11-Rad50-Xrs2 to DNA end resection, Proc. Natl. Acad. Sci. U. S. A. 110 (2013) E1661–E1668.

[59] R. Anand, L. Ranjha, E. Cannavo, P. Cejka, Phosphorylated CtIP functions as a Co-factor of the MRE11-RAD50-NBS1 endonuclease in DNA end resection, Mol Cell 64 (2016) 940–950.

[60] F. Persson, J.O. Tegenfeldt, DNA in nanochannels—directly visualizing genomic information, Chem. Soc. Rev. 39 (2010) 985.

[61] G. Goyal, et al., A simple cut and stretch assay to detect antimicrobial resistance genes on bacterial plasmids by single-molecule fluorescence microscopy, Sci. Rep. 12 (2022) 9301.

[62] V. Singh, P. Johansson, Y.-L. Lin, O. Hammarsten, F. Westerlund, Shining light on single-strand lesions caused by the chemotherapy drug bleomycin, DNA Repair 105 (2021) 103153.

[63] T. Chatterjee, A. Johnson-Buck, N.G. Walter, Highly sensitive protein detection by aptamer-based single-molecule kinetic fingerprinting, Biosens. Bioelectron. 216 (2022).

[64] M. Levy, S.F. Cater, A.D. Ellington, Quantum-dot aptamer beacons for the detection of proteins, Chembiochem 6 (2005) 2163–2166.

[65] S. Wu, et al., An ssDNA aptamer specific for detection and purification of hexahistidine-tagged proteins, Anal. Biochem. 607 (2020) 113893.

[66] K. Frykholm, et al., Fast size-determination of intact bacterial plasmids using nanofluidic channels, Lab Chip 15 (2015) 2739–2743.

[67] E. Cannavo, P. Cejka, Sae2 promotes dsDNA endonuclease activity within Mre11–Rad50–Xrs2 to resect DNA breaks, Nature 514 (2014) 122–125.

[68] M. Alizadehheidari, et al., Nanoconfined circular and linear DNA: equilibrium conformations and unfolding kinetics, Macromolecules 48 (2015) 871–878.

[69] K. Frykholm, et al., Fast size-determination of intact bacterial plasmids using nanofluidic channels, Lab Chip 15 (2015) 2739–2743.

[70] Y. Liu, et al., ATP-dependent DNA binding, unwinding, and resection by the Mre11/Rad50 complex, EMBO J. 35 (2016) 743–758.

[71] H.S. Lim, J.S. Kim, Y.B. Park, G.H. Gwon, Y. Cho, Crystal structure of the mre11-rad50-ATPγS complex: understanding the interplay between Mre11 and Rad50, Genes Dev. 25 (2011) 1091–1104.

[72] L. Ranjha, S.M. Howard, P. Cejka, Main steps in DNA double-strand break repair: an introduction to homologous recombination and related processes, Chromosoma 127 (2018) 187–214.

[73] K. Jiang, et al., The HIV-1 nucleocapsid chaperone protein forms locally compacted globules on long double-stranded DNA, Nucleic Acids Res. 49 (2021) 4550–4563.

[74] J. Krog, et al., Stochastic unfolding of nanoconfined DNA: experiments, model and Bayesian analysis, J. Chem. Phys. 149 (2018) 215101.

[75] M. Roushan, et al., Probing transient protein-mediated DNA linkages using nanoconfinement, Biomicrofluidics 8 (2014) 034113.

[76] D. Nakada, K. Matsumoto, K. Sugimoto, ATM-related Tel1 associates with double-strand breaks through an Xrs2-dependent mechanism, Genes Dev. 17 (2003) 1957–1962.

[77] Z.-W. Zhou, et al., NBS1 interacts with Notch signaling in neuronal homeostasis, Nucleic Acids Res. 48 (2020) 10924–10939.

[78] R.S. Williams, et al., Nbs1 flexibly tethers Ctp1 and mre11-rad50 to coordinate DNA double-strand break processing and repair, Cell 139 (2009) 87–99.

[79] L.H. Fornander, et al., Visualizing the nonhomogeneous structure of RAD51 filaments using nanofluidic channels, Langmuir 32 (2016) 8403–8412.